Computers and Structures 191 (2017) 22–32

Contents lists available at ScienceDirect

Computers and Structures

journal homepage: www.elsevier.com/locate/compstruc

Improving the accuracy of the dual Craig-Bampton method

Jeong-Ho Kim [a], Jaemin Kim [b], Phill-Seung Lee [a,*]

[a] Department of Mechanical Engineering, Korea Advanced Institute of Science and Technology, 291 Daehak-ro, Yuseong-gu, Daejeon 34141, Republic of Korea
[b] Civil Business Unit, Engineering & Construction Group, Samsung C&T Corporation, 145 Pangyoyeok-ro, Bundang-gu, Seongnam-si, Gyeonggi-do 13530, Republic of Korea

ARTICLE INFO

Article history:
Received 17 January 2017
Accepted 25 May 2017

Keywords:
Structural dynamics
Finite element method
Model reduction
Component mode synthesis
Dual Craig-Bampton method
Residual flexibility
Interface reduction

ABSTRACT

The objective of the work reported in this paper is to improve the well-known dual Craig-Bampton (DCB) method. The original transformation matrix of the DCB method is enhanced by considering the higher-order effect of residual substructural modes through residual flexibility. Using the new transformation matrix, original finite element models can be more accurately approximated in the reduced models. Herein, additional generalized coordinates are newly defined for considering the 2nd order residual flexibility. Additional coordinates related to the interface boundary can be eliminated by applying the concept of SEREP (the system equivalent reduction expansion process). The formulation of the improved DCB method is presented in detail, and its accuracy is investigated through numerical examples.

1. Introduction

In engineering practice, the degrees of freedom (DOFs) of numerical models have been continuously increased, along with the rapid increase in their complexity. When a complicated structure consisting with diverse components is designed through the cooperation of different engineers, it is very expensive to deal with its finite element models. This is because frequent design modifications affecting the whole and component models require repeated reanalysis. For these reasons, a number of model-reduction schemes have spotlighted its necessity, especially, in the structural dynamics community [1–36,40]. Among the proposed solutions, component mode synthesis (CMS) methods are considered very powerful solutions. With CMS methods, a large structural model is represented by an assemblage of small substructures; then is approximated using a reduced model constructed using only the dominant substructural modes. In CMS methods, it is important to select the proper dominant modes [2–4].

After pioneering work by Hurty [1] in the 1960s, numerous CMS methods have been introduced for various applications [5–34]. The CMS methods can be classified as fixed, free, and mixed-interface based methods, depending on how the interface is handled. The most successful fixed-interface based method is the Craig-Bampton method (CB method) [5] due to its simplicity, robustness, and accuracy. In contrast, the free-interface based methods [7–9] proposed earlier were not successful because those methods were not adequate for either accuracy or efficiency in spite of their important advantages. These included such as substructural independence and easy treatment of various interface conditions [9,20–22].

In 2004, Rixen [11] introduced a new free-interface based method as a dual counterpart of the CB method, namely, the dual Craig-Bampton (DCB) method. In the DCB method, Lagrange multipliers are employed along the interface for assembling substructures and thus an original assembled finite element (FE) model can be effectively reduced as a form of quasi-diagonal matrices, leading to computational efficiency. The most advantageous feature of the DCB method is that, when a substructure is changed, entire reduced matrices do not need be updated again because in the formulation, substructures are handled independently. This feature also makes it possible to assemble substructures even if their FE meshes do not match along the interface [16]. For all these reasons, the DCB method is an attractive solution for experimental-FE model correlation [17–19], as well as FE model updating and dynamic analysis considering various constraint conditions (contact, connection joint, damage, etc.) [20–22]. However, the DCB method still needs improvement in accuracy. In particular, the DCB method causes a weakening of the interface compatibility in reduced models, resulting in spurious modes with negative eigenvalues [11,14]. If the reduction basis chosen is not sufficient, such spurious modes may occur in lower modes, which is an obstacle to approximating the original FE model correctly.

* Corresponding author.
E-mail address: phillseung@kaist.edu (P.-S. Lee).

http://dx.doi.org/10.1016/j.compstruc.2017.05.010
0045-7949/

Recently, fixed-interface based CMS methods have been successfully improved considering the higher-order effect of the residual modes [10,24,25,29,30]. The motivation of this study is that the same principle can be adopted for improving free-interface based methods. In this study, we focus on improving the accuracy of the DCB method. We derive a new transformation matrix for the DCB method, improved by considering the 2nd order effect of residual substructural modes. One difficulty comes from the fact that the improved approximation of substructural dynamic behavior contains unknown eigenvalues. In the formulation, unknown eigenvalues are considered additional generalized coordinates. These are subsequently eliminated using the concept of the system equivalent reduction expansion process (SEREP) to reduce computational cost. Finally, improved solution-accuracy is obtained in the final reduced systems. Furthermore, the use of the present method avoids creation of spurious modes with negative eigenvalues in the lower modes.

In Section 2, we briefly review the original DCB method; and formulation of the improved DCB method is presented in Section 3. Section 4 describes the performance of the improved DCB method through various numerical examples and in Section 5, we explore the negative eigenvalues in lower modes for the original and improved DCB methods. Finally, conclusions are presented in Section 6.

2. Dual Craig-Bampton method

In this section, we briefly introduce the formulation of the dual Craig-Bampton (DCB) method, see Refs. [11,14,20,31] for detailed derivations.

In the DCB method, a structural FE model is assembled by N_s substructures as in Fig. 1a. The substructures are connected through a free interface boundary Γ (Fig. 1b). The compatibility between substructures is explicitly enforced using the following constraint equation

$$\sum_{i=1}^{N_s} \mathbf{b}^{(i)^T} \mathbf{u}_b^{(i)} = \mathbf{0}, \tag{1}$$

in which $\mathbf{u}_b^{(i)}$ is the interface displacement vector of the i-th substructure, and $\mathbf{b}^{(i)}$ is a signed Boolean matrix.

The linear dynamic equations for each substructure Ω_i can be individually expressed by

$$\mathbf{M}^{(i)}\ddot{\mathbf{u}}^{(i)} + \mathbf{K}^{(i)}\mathbf{u}^{(i)} + \mathbf{B}^{(i)}\boldsymbol{\mu} = \mathbf{f}^{(i)}, \quad i = 1, \cdots, N_s, \tag{2}$$

where $\mathbf{M}^{(i)}$ and $\mathbf{K}^{(i)}$ are the mass and stiffness matrices of the i-th substructure, $\mathbf{u}^{(i)}$ is the corresponding displacement vector, $\mathbf{f}^{(i)}$ is the external load vector applied to the substructure, and $\mathbf{B}^{(i)}\boldsymbol{\mu}$ is the interconnecting force between substructures with $\mathbf{B}^{(i)} = \begin{bmatrix} \mathbf{0} \\ \mathbf{b}^{(i)} \end{bmatrix}$ and the Lagrange multiplier vector $\boldsymbol{\mu}$. Note that $\ddot{()} = d^2()/dt^2$ with time variable t.

Assembling the linear dynamic equations for each substructure in Eq. (2) using the compatibility constraint equation in Eq. (1), the dynamic equilibrium equation of the original assembled FE model (see Fig. 1c) is constructed as

$$\begin{bmatrix} \mathbf{M} & \mathbf{0} \\ \mathbf{0} & \mathbf{0} \end{bmatrix} \begin{bmatrix} \ddot{\mathbf{u}} \\ \boldsymbol{\mu} \end{bmatrix} + \begin{bmatrix} \mathbf{K} & \mathbf{B} \\ \mathbf{B}^T & \mathbf{0} \end{bmatrix} \begin{bmatrix} \mathbf{u} \\ \boldsymbol{\mu} \end{bmatrix} = \begin{bmatrix} \mathbf{f} \\ \mathbf{0} \end{bmatrix}, \tag{3}$$

with $\mathbf{M} = \begin{bmatrix} \mathbf{M}^{(1)} & & \mathbf{0} \\ & \ddots & \\ \mathbf{0} & & \mathbf{M}^{(N_s)} \end{bmatrix}$, $\mathbf{K} = \begin{bmatrix} \mathbf{K}^{(1)} & & \mathbf{0} \\ & \ddots & \\ \mathbf{0} & & \mathbf{K}^{(N_s)} \end{bmatrix}$, $\mathbf{u} = \begin{bmatrix} \mathbf{u}^{(1)} \\ \vdots \\ \mathbf{u}^{(N_s)} \end{bmatrix}$, $\mathbf{f} = \begin{bmatrix} \mathbf{f}^{(1)} \\ \vdots \\ \mathbf{f}^{(N_s)} \end{bmatrix}$, $\mathbf{B} = \begin{bmatrix} \mathbf{B}^{(1)} \\ \vdots \\ \mathbf{B}^{(N_s)} \end{bmatrix}$, where $\mathbf{M}$ and $\mathbf{K}$ are block-diagonal mass and stiffness matrices that consist of substructural mass and stiffness matrices ($\mathbf{M}^{(i)}$ and $\mathbf{K}^{(i)}$).

The global eigenvalue problem is defined for the original assembled FE model

$$\mathbf{K}_g(\boldsymbol{\varphi}_g)_i = (\lambda_g)_i \mathbf{M}_g(\boldsymbol{\varphi}_g)_i \quad \text{for } i = 1, \cdots, N_g, \tag{4}$$

with $\mathbf{K}_g = \begin{bmatrix} \mathbf{K} & \mathbf{B} \\ \mathbf{B}^T & \mathbf{0} \end{bmatrix}$, $\mathbf{M}_g = \begin{bmatrix} \mathbf{M} & \mathbf{0} \\ \mathbf{0} & \mathbf{0} \end{bmatrix}$, in which $(\lambda_g)_i$ and $(\boldsymbol{\varphi}_g)_i$ are the global eigenvalue and eigenvector corresponding to the i-th global mode, respectively, and N_g is the number of DOFs in the original FE model. This number consists of interface and substructural DOFs ($N_g = N_b + \sum_{i=1}^{N_s} N_u^{(i)}$, where N_b is the number of interface DOFs and $N_u^{(i)}$ is the number of DOFs of the i-th substructure).

Because each substructure can be seen as being excited through interconnecting forces, the displacement of each substructure is assumed in the original DCB formulation, as

$$\mathbf{u}^{(i)} \approx -\mathbf{K}^{(i)^+}\mathbf{B}^{(i)}\boldsymbol{\mu} + \mathbf{R}^{(i)}\boldsymbol{\alpha}^{(i)} + \boldsymbol{\Theta}^{(i)}\mathbf{q}^{(i)}, \; i = 1, \cdots, N_s, \tag{5}$$

where $\mathbf{K}^{(i)^+}$ is the generalized inverse matrix of $\mathbf{K}^{(i)}$ (the flexibility matrix), $\mathbf{R}^{(i)}$ is the rigid body mode matrix, $\boldsymbol{\Theta}^{(i)}$ is the matrix that consists of free interface normal modes, and $\boldsymbol{\alpha}^{(i)}$ and $\mathbf{q}^{(i)}$ are the corresponding generalized coordinate vectors.

The rigid body and free interface normal modes of the i-th substructure are calculated by solving the following eigenvalue problems

$$\mathbf{K}^{(i)}(\boldsymbol{\varphi}^{(i)})_j = \lambda_j^{(i)}\mathbf{M}^{(i)}(\boldsymbol{\varphi}^{(i)})_j, \; j = 1, \cdots, N_u^{(i)}, \tag{6}$$

in which $\lambda_j^{(i)}$ and $(\boldsymbol{\varphi}^{(i)})_j$ are the j-th eigenvalue and the corresponding mode, respectively. Note that the mode vectors are scaled to satisfy the mass-orthonormality condition.

The free interface normal mode matrix $\boldsymbol{\Theta}^{(i)}$ in Eq. (5) consists of dominant and residual normal modes

$$\boldsymbol{\Theta}^{(i)} = \begin{bmatrix} \boldsymbol{\Theta}_d^{(i)} & \boldsymbol{\Theta}_r^{(i)} \end{bmatrix}, \tag{7}$$

in which $\boldsymbol{\Theta}_d^{(i)}$ and $\boldsymbol{\Theta}_r^{(i)}$ includes $N_d^{(i)}$ dominant free interface normal modes, and the remaining modes, respectively.

The displacement of the substructure can be approximated using only the dominant modes

$$\mathbf{u}^{(i)} \approx -\mathbf{K}^{(i)^+}\mathbf{B}^{(i)}\boldsymbol{\mu} + \mathbf{R}^{(i)}\boldsymbol{\alpha}^{(i)} + \boldsymbol{\Theta}_d^{(i)}\mathbf{q}_d^{(i)}, \tag{8}$$

where the term $-\mathbf{K}^{(i)^+}\mathbf{B}^{(i)}\boldsymbol{\mu}$ is the static displacement by interconnecting forces, and this term can be expressed using modal parameters

$$-\mathbf{K}^{(i)^+}\mathbf{B}^{(i)}\boldsymbol{\mu} = -\boldsymbol{\Theta}^{(i)}\boldsymbol{\Lambda}^{(i)^{-1}}\boldsymbol{\Theta}^{(i)^T}\mathbf{B}^{(i)}\boldsymbol{\mu} \quad \text{with}$$
$$\boldsymbol{\Lambda}^{(i)} = \text{diag}\left(\lambda_1^{(i)}, \lambda_2^{(i)}, \ldots \lambda_{N_u^{(i)}}^{(i)}\right), \tag{9}$$

where $\boldsymbol{\Lambda}^{(i)}$ is the substructural eigenvalue matrix.

Substituting Eq. (7) into Eq. (9), the static displacement can be divided into dominant and residual parts

$$-\mathbf{K}^{(i)^+}\mathbf{B}^{(i)}\boldsymbol{\mu} = -\boldsymbol{\Theta}_d^{(i)}\boldsymbol{\Lambda}_d^{(i)^{-1}}\boldsymbol{\Theta}_d^{(i)^T}\mathbf{B}^{(i)}\boldsymbol{\mu} - \boldsymbol{\Theta}_r^{(i)}\boldsymbol{\Lambda}_r^{(i)^{-1}}\boldsymbol{\Theta}_r^{(i)^T}\mathbf{B}^{(i)}\boldsymbol{\mu}, \tag{10}$$

with the corresponding substructural eigenvalue matrices $\boldsymbol{\Lambda}_d^{(i)}$ and $\boldsymbol{\Lambda}_r^{(i)}$ defined by

$$\boldsymbol{\Lambda}_d^{(i)} = \boldsymbol{\Theta}_d^{(i)^T}\mathbf{K}^{(i)}\boldsymbol{\Theta}_d^{(i)}, \; \boldsymbol{\Lambda}_r^{(i)} = \boldsymbol{\Theta}_r^{(i)^T}\mathbf{K}^{(i)}\boldsymbol{\Theta}_r^{(i)}. \tag{11}$$

Using Eq. (10) in Eq. (8), the following equation is obtained:

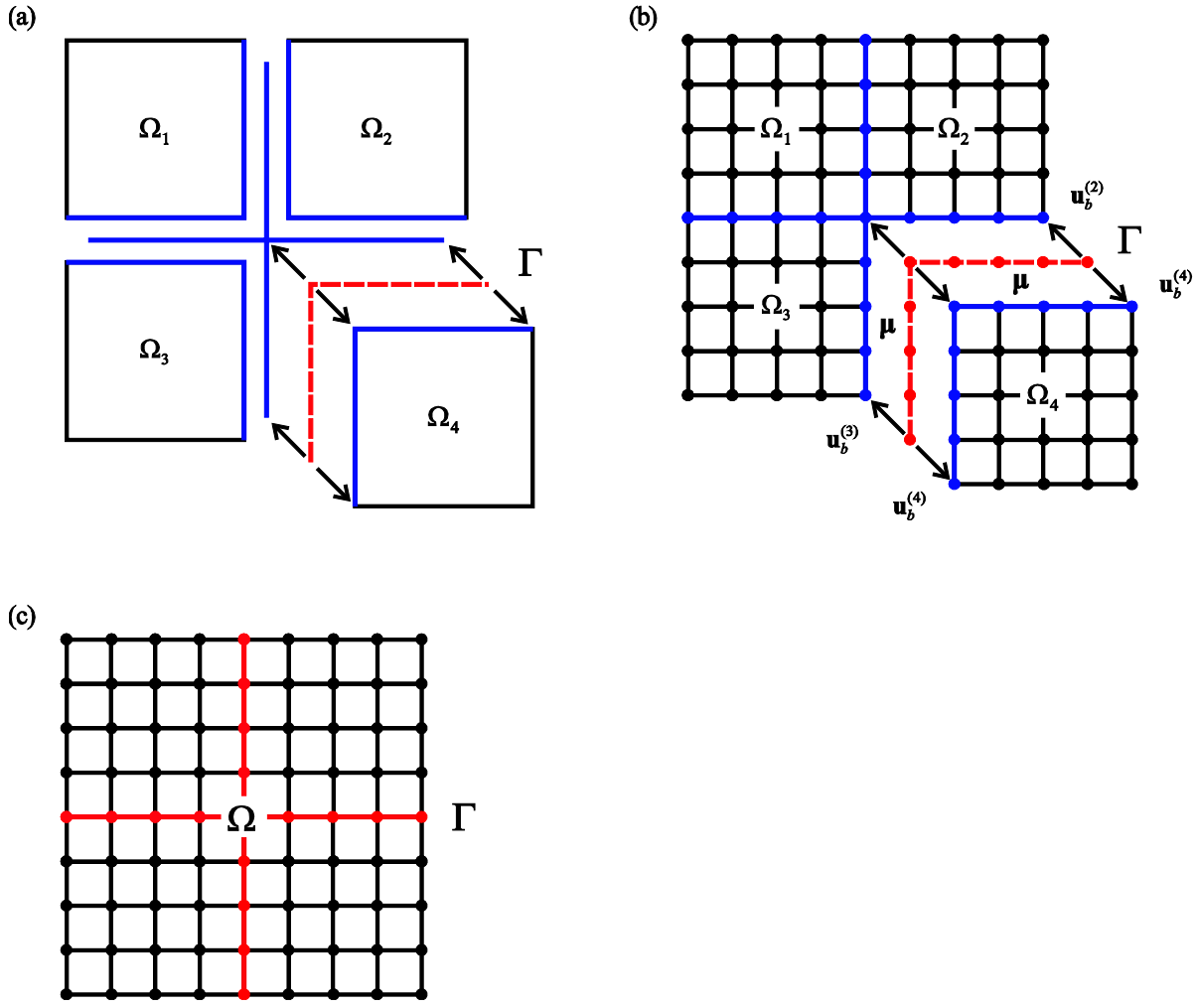

Fig. 1. Assemblage of substructures and interface handling in the DCB method ($N_s = 4$). (a) Substructures, Ω_1, Ω_2, Ω_3 and Ω_4, (b) Interconnecting forces and interfacial DOFs of the substructure Ω_4, (c) Assembled FE model Ω with its interface boundary Γ.

$$\mathbf{u}^{(i)} \approx -\boldsymbol{\Theta}_d^{(i)}\boldsymbol{\Lambda}_d^{(i)^{-1}}\boldsymbol{\Theta}_d^{(i)^T}\mathbf{B}^{(i)}\boldsymbol{\mu} - \boldsymbol{\Theta}_r^{(i)}\boldsymbol{\Lambda}_r^{(i)^{-1}}\boldsymbol{\Theta}_r^{(i)^T}\mathbf{B}^{(i)}\boldsymbol{\mu} + \mathbf{R}^{(i)}\boldsymbol{\alpha}^{(i)} + \boldsymbol{\Theta}_d^{(i)}\mathbf{q}_d^{(i)}. \tag{12}$$

It is easily observed that the first and last terms on the right side of Eq. (12) are identical and thus neglecting the first term, we obtain

$$\mathbf{u}^{(i)} \approx -\mathbf{F}_1^{(i)}\mathbf{B}^{(i)}\boldsymbol{\mu} + \mathbf{R}^{(i)}\boldsymbol{\alpha}^{(i)} + \boldsymbol{\Theta}_d^{(i)}\mathbf{q}_d^{(i)} \quad \text{with } \mathbf{F}_1^{(i)} = \boldsymbol{\Theta}_r^{(i)}\boldsymbol{\Lambda}_r^{(i)^{-1}}\boldsymbol{\Theta}_r^{(i)^T}. \tag{13}$$

in which $\mathbf{F}_1^{(i)}$ is called the residual flexibility matrix. The residual flexibility matrix can be calculated by subtracting the dominant flexibility matrix from the full flexibility matrix $\mathbf{K}^{(i)^+}$

$$\mathbf{F}_1^{(i)} = \mathbf{K}^{(i)^+} - \boldsymbol{\Theta}_d^{(i)}\boldsymbol{\Lambda}_d^{(i)^{-1}}\boldsymbol{\Theta}_d^{(i)^T}. \tag{14}$$

The displacement and the Lagrange multipliers of the i-th substructure can be approximated using the transformation

$$\begin{bmatrix}\mathbf{u}^{(i)}\\ \boldsymbol{\mu}\end{bmatrix} \approx \mathbf{T}_1^{(i)}\begin{bmatrix}\boldsymbol{\alpha}^{(i)}\\ \mathbf{q}_d^{(i)}\\ \hdashline \boldsymbol{\mu}\end{bmatrix} \quad \text{with} \quad \mathbf{T}_1^{(i)} = \left[\begin{array}{cc:c}\mathbf{R}^{(i)} & \boldsymbol{\Theta}_d^{(i)} & -\mathbf{F}_1^{(i)}\mathbf{B}^{(i)}\\ \mathbf{0} & \mathbf{0} & \mathbf{I}\end{array}\right], \tag{15}$$

in which $\mathbf{T}_1^{(i)}$ is the substructural transformation matrix of the original DCB method for the i -th substructure. Note that, in the substurctural eigenvalue problem, only the eigenpairs of the dominant and rigid body modes are calculated, not for all eigenpairs.

The transformation matrix $\mathbf{T}_1$ ($N_g \times N_1$) for the original assembled FE model is then given by

$$\begin{bmatrix}\mathbf{u}\\ \boldsymbol{\mu}\end{bmatrix} \approx \mathbf{T}_1\begin{bmatrix}\boldsymbol{\alpha}^{(1)}\\ \vdots\\ \boldsymbol{\alpha}^{(N_s)}\\ \mathbf{q}_d^{(1)}\\ \vdots\\ \mathbf{q}_d^{(N_s)}\\ \hdashline \boldsymbol{\mu}\end{bmatrix} \text{ with}$$

$$\mathbf{T}_1 = \left[\begin{array}{ccccccc:c}\mathbf{R}^{(1)} & & \mathbf{0} & \boldsymbol{\Theta}_d^{(1)} & & \mathbf{0} & -\mathbf{F}_1^{(1)}\mathbf{B}^{(1)}\\ & \ddots & & & \ddots & & \vdots\\ \mathbf{0} & & \mathbf{R}^{(N_s)} & \mathbf{0} & & \boldsymbol{\Theta}_d^{(N_s)} & -\mathbf{F}_1^{(N_s)}\mathbf{B}^{(N_s)}\\ \mathbf{0} & \cdots & \mathbf{0} & \mathbf{0} & \cdots & \mathbf{0} & \mathbf{I}\end{array}\right]. \tag{16}$$

and the reduced mass and stiffness matrices ($N_1 \times N_1$) and the force vector ($N_1 \times 1$) are obtained using the transformation matrix

$$\bar{\mathbf{M}}_1 = \mathbf{T}_1^T \begin{bmatrix} \mathbf{M} & \mathbf{0} \\ \mathbf{0} & \mathbf{0} \end{bmatrix} \mathbf{T}_1,\ \bar{\mathbf{K}}_1 = \mathbf{T}_1^T \begin{bmatrix} \mathbf{K} & \mathbf{B} \\ \mathbf{B}^T & \mathbf{0} \end{bmatrix} \mathbf{T}_1, \bar{\mathbf{f}}_1 = \mathbf{T}_1^T \begin{bmatrix} \mathbf{f} \\ \mathbf{0} \end{bmatrix}. \tag{17}$$

Note that N_1 is the number of DOFs in the reduced FE model: $N_1 = N_0 + N_b$ with $N_0 = \sum_{i=1}^{N_s} (N_r^{(i)} + N_d^{(i)})$, in which $N_r^{(i)}$ and $N_d^{(i)}$ are the numbers of rigid body modes and dominant modes of the i -th substructure, respectively.

3. Improved dual Craig-Bampton method

In the original DCB method, to construct the transformation matrix $\mathbf{T}_1$ in Eq. (16), the residual substructural modes are considered through the static flexibility matrix $\mathbf{K}^{(i)^+}$. However, in order to improve the DCB method, we here properly consider the effect of the residual substructural modes using dynamic flexibility, resulting in improved solution accuracy in the reduced models.

3.1. Second order dynamic residual flexibility

Let us consider Eq. (2) with $\mathbf{f}^{(i)} = \mathbf{0}$, and invoking harmonic response ($d^2/dt^2 = -\lambda$). The displacement of the i-th substructure can be written as

$$\mathbf{u}^{(i)} = -(\mathbf{K}^{(i)} - \lambda \mathbf{M}^{(i)})^{-1} \mathbf{B}^{(i)} \boldsymbol{\mu},\ i = 1, \cdots, N_s, \tag{18}$$

in which $(\mathbf{K}^{(i)} - \lambda \mathbf{M}^{(i)})^{-1}$ is called the dynamic flexibility matrix. Using free interface normal modes and rigid body modes obtained from Eq. (6), the dynamic flexibility matrix can be rewritten in terms of modal parameters

$$(\mathbf{K}^{(i)} - \lambda \mathbf{M}^{(i)})^{-1} = \boldsymbol{\Phi}^{(i)} (\boldsymbol{\Lambda}^{(i)} - \lambda \mathbf{I}^{(i)})^{-1} \boldsymbol{\Phi}^{(i)^T} \text{ with } \boldsymbol{\Phi}^{(i)} = \begin{bmatrix} \boldsymbol{\Theta}^{(i)} & \mathbf{R}^{(i)} \end{bmatrix}. \tag{19}$$

Substituting Eq. (19) into Eq. (18), the substructural displacement is represented by

$$\mathbf{u}^{(i)} = -\boldsymbol{\Theta}^{(i)} (\boldsymbol{\Lambda}_n^{(i)} - \lambda \mathbf{I}_n^{(i)})^{-1} \boldsymbol{\Theta}^{(i)^T} \mathbf{B}^{(i)} \boldsymbol{\mu} + \mathbf{R}^{(i)} \boldsymbol{\alpha}^{(i)} \tag{20}$$

with $\boldsymbol{\Lambda}_n^{(i)} = \boldsymbol{\Theta}^{(i)^T} \mathbf{K}^{(i)} \boldsymbol{\Theta}^{(i)}$, $\mathbf{I}_n^{(i)} = \boldsymbol{\Theta}^{(i)^T} \mathbf{M}^{(i)} \boldsymbol{\Theta}^{(i)}$, in which $\boldsymbol{\Lambda}_n^{(i)}$ and $\mathbf{I}_n^{(i)}$ are the eigenvalue and identity matrices corresponding to the free interface normal modes, and λ is the unknown eigenvalue.

We then substitute Eq. (7) into Eq. (20), to obtain

$$\mathbf{u}^{(i)} = \boldsymbol{\Theta}_d^{(i)} \mathbf{q}_d^{(i)} - \boldsymbol{\Theta}_r^{(i)} (\boldsymbol{\Lambda}_r^{(i)} - \lambda \mathbf{I}_r^{(i)})^{-1} \boldsymbol{\Theta}_r^{(i)^T} \mathbf{B}^{(i)} \boldsymbol{\mu} + \mathbf{R}^{(i)} \boldsymbol{\alpha}^{(i)} \tag{21}$$

with $\boldsymbol{\Theta}_d^{(i)} \mathbf{q}_d^{(i)} = -\boldsymbol{\Theta}_d^{(i)} (\boldsymbol{\Lambda}_d^{(i)} - \lambda \mathbf{I}_d^{(i)})^{-1} \boldsymbol{\Theta}_d^{(i)^T} \mathbf{B}^{(i)} \boldsymbol{\mu}$.

In Eq. (21), the residual part of the dynamic flexibility matrix $\boldsymbol{\Theta}_r^{(i)} (\boldsymbol{\Lambda}_r^{(i)} - \lambda \mathbf{I}_r^{(i)})^{-1} \boldsymbol{\Theta}_r^{(i)^T}$ can be expanded using a Taylor series [10,13,15,24–29]

$$\boldsymbol{\Theta}_r^{(i)} (\boldsymbol{\Lambda}_r^{(i)} - \lambda \mathbf{I}_r^{(i)})^{-1} \boldsymbol{\Theta}_r^{(i)^T} = \mathbf{F}_1^{(i)} + \lambda \mathbf{F}_2^{(i)} + \cdots \lambda^{j-1} \mathbf{F}_j^{(i)} + \cdots \text{ with}$$
$$\mathbf{F}_j^{(i)} = \boldsymbol{\Theta}_r^{(i)} \boldsymbol{\Lambda}_r^{(i)^{-j}} \boldsymbol{\Theta}_r^{(i)^T}, \tag{22}$$

where $\mathbf{F}_j^{(i)}$ is the j-th order residual flexibility matrix of the i-th substructure.

Considering the residual flexibility up to the 2nd order, the residual part of the dynamic flexibility matrix is approximated by

$$\boldsymbol{\Theta}_r^{(i)} (\boldsymbol{\Lambda}_r^{(i)} - \lambda \mathbf{I}_r^{(i)})^{-1} \boldsymbol{\Theta}_r^{(i)^T} \approx \mathbf{F}_1^{(i)} + \lambda \mathbf{F}_2^{(i)}, \tag{23}$$

and using Eq. (23) in Eq. (21), the substructural displacement is expressed as

$$\mathbf{u}^{(i)} \approx \boldsymbol{\Theta}_d^{(i)} \mathbf{q}_d^{(i)} - \mathbf{F}_1^{(i)} \mathbf{B}^{(i)} \boldsymbol{\mu} - \lambda \mathbf{F}_2^{(i)} \mathbf{B}^{(i)} \boldsymbol{\mu} + \mathbf{R}^{(i)} \boldsymbol{\alpha}^{(i)}. \tag{24}$$

Note that the substructural displacement of the original DCB formulation is obtained when the 2nd order residual flexibility in Eq. (24) is ignored. The added 2nd order residual flexibility contributes to strengthening the interface compatibility by more precisely calculating the displacement due to the interconnecting forces. As a result, it is expected that the emergence of spurious modes can be avoided in the lower modes. This feature will be briefly demonstrated using a numerical example. The 2nd order residual flexibility matrix can be easily calculated by reusing $\mathbf{F}_1^{(i)}$ in Eq. (14)

$$\mathbf{F}_2^{(i)} = \mathbf{F}_1^{(i)} \mathbf{M}^{(i)} \mathbf{F}_1^{(i)}. \tag{25}$$

The substructural transformation matrix $\bar{\mathbf{T}}_2^{(i)}$ with the 2nd order residual flexibility approximation is given by

$$\begin{bmatrix} \mathbf{u}^{(i)} \\ \boldsymbol{\mu} \end{bmatrix} \approx \bar{\mathbf{T}}_2^{(i)} \mathbf{u}_2^{(i)}, \tag{26}$$

$$\text{with } \bar{\mathbf{T}}_2^{(i)} = \left[\begin{array}{cc:cc} \mathbf{R}^{(i)} & \boldsymbol{\Theta}_d^{(i)} & -\mathbf{F}_1^{(i)} \mathbf{B}^{(i)} & \bar{\boldsymbol{\Theta}}_2^{(i)} \\ \mathbf{0} & \mathbf{0} & \mathbf{I} & \mathbf{0} \end{array}\right],\ \mathbf{u}_2^{(i)} = \begin{bmatrix} \boldsymbol{\alpha}^{(i)} \\ \mathbf{q}_d^{(i)} \\ \hdashline \boldsymbol{\mu} \\ \boldsymbol{\psi} \end{bmatrix},\ \bar{\boldsymbol{\Theta}}_2^{(i)} = -\mathbf{F}_2^{(i)} \mathbf{B}^{(i)},$$

$\boldsymbol{\psi} = \lambda \boldsymbol{\mu}$, where $\mathbf{u}_2^{(i)}$ denotes the generalized coordinate vector and $\boldsymbol{\psi}$ is the additional coordinate vector containing the unknown eigenvalue λ .

It is important to note that the use of higher-order residual flexibility may produce badly scaled transformation matrices, resulting in ill-conditioned reduced system matrices. Thus, we normalize each column of $\bar{\boldsymbol{\Theta}}_2^{(i)}$ using its L2-norm [37,38].

$$\boldsymbol{\Theta}_2^{(i)} = \bar{\boldsymbol{\Theta}}_2^{(i)} \mathbf{G}^{(i)^{-1}} \text{ with } \mathbf{G}^{(i)} = \begin{bmatrix} \|\{\bar{\boldsymbol{\theta}}_2^{(i)}\}_1\|_2 & & & \mathbf{0} \\ & \|\{\bar{\boldsymbol{\theta}}_2^{(i)}\}_2\|_2 & & \\ & & \ddots & \\ \mathbf{0} & & & \|\{\bar{\boldsymbol{\theta}}_2^{(i)}\}_{N_b}\|_2 \end{bmatrix}, \tag{27}$$

where $\boldsymbol{\Theta}_2^{(i)}$ is the normalized residual mode matrix containing the 2nd order residual flexibility, and $\{\bar{\boldsymbol{\theta}}_2^{(i)}\}_j$ is the j-th column vector of $\bar{\boldsymbol{\Theta}}_2^{(i)}$.

Substituting Eq. (27) into Eq. (26), the substructural transformation matrix of the improved DCB method for the i-th substructure is

$$\begin{bmatrix} \mathbf{u}^{(i)} \\ \boldsymbol{\mu} \end{bmatrix} \approx \mathbf{T}_2^{(i)} \mathbf{u}_2^{(i)} \quad \text{with} \quad \mathbf{T}_2^{(i)} = \left[\begin{array}{cc:cc} \mathbf{R}^{(i)} & \boldsymbol{\Theta}_d^{(i)} & -\mathbf{F}_1^{(i)} \mathbf{B}^{(i)} & \boldsymbol{\Theta}_2^{(i)} \\ \mathbf{0} & \mathbf{0} & \mathbf{I} & \mathbf{0} \end{array}\right]. \tag{28}$$

Then, the displacement and Lagrange multipliers of the original assembled FE model with N_s substructures are approximated as

$$\begin{bmatrix} \mathbf{u} \\ \boldsymbol{\mu} \end{bmatrix} \approx \mathbf{T}_2 \begin{bmatrix} \boldsymbol{\alpha}^{(1)} \\ \vdots \\ \boldsymbol{\alpha}^{(N_s)} \\ \mathbf{q}_d^{(1)} \\ \vdots \\ \mathbf{q}_d^{(N_s)} \\ \hdashline \boldsymbol{\mu} \\ \boldsymbol{\psi} \end{bmatrix} \text{ with}$$

$$\mathbf{T}_2 = \begin{bmatrix} \mathbf{R}^{(1)} & & \mathbf{0} & \boldsymbol{\Theta}_d^{(1)} & & \mathbf{0} & -\mathbf{F}_1^{(1)}\mathbf{B}^{(1)} & \boldsymbol{\Theta}_2^{(1)} \\ & \ddots & & & \ddots & & \vdots & \vdots \\ \mathbf{0} & & \mathbf{R}^{(N_s)} & \mathbf{0} & & \boldsymbol{\Theta}_d^{(N_s)} & -\mathbf{F}_1^{(N_s)}\mathbf{B}^{(N_s)} & \boldsymbol{\Theta}_2^{(N_s)} \\ \mathbf{0} & \cdots & \mathbf{0} & \mathbf{0} & \cdots & \mathbf{0} & \mathbf{I} & \mathbf{0} \end{bmatrix} \tag{29}$$

Using the transformation matrix $\mathbf{T}_2$ $(N_g \times N_2)$ in Eq. (29), the reduced system matrices $(N_2 \times N_2)$ and force vector $(N_2 \times 1)$ are calculated

$$\bar{\mathbf{M}}_2 = \mathbf{T}_2^T \begin{bmatrix} \mathbf{M} & \mathbf{0} \\ \mathbf{0} & \mathbf{0} \end{bmatrix} \mathbf{T}_2, \; \bar{\mathbf{K}}_2 = \mathbf{T}_2^T \begin{bmatrix} \mathbf{K} & \mathbf{B} \\ \mathbf{B}^T & \mathbf{0} \end{bmatrix} \mathbf{T}_2, \bar{\mathbf{f}}_2 = \mathbf{T}_2^T \begin{bmatrix} \mathbf{f} \\ \mathbf{0} \end{bmatrix}, \tag{30}$$

in which $\bar{\mathbf{M}}_2$, $\bar{\mathbf{K}}_2$, and $\bar{\mathbf{f}}_2$ are the reduced mass and stiffness matrices, and the reduced force vector, respectively. Note that N_2 is the number of DOFs in the reduced FE model, $N_2 = 2N_b + \sum_{i=1}^{N_s}(N_r^{(i)} + N_d^{(i)})$.

3.2. Interface reduction

When the 2nd order residual flexibility is considered, the size of reduced system is increased due to the additional coordinates $\boldsymbol{\psi}$ compared to the original DCB method. The number of increased DOFs is equal to the number of interfacial DOFs.

To resolve this problem, we eliminate the additional coordinates by employing the concept of the system equivalent reduction expansion process (SEREP) [36]. In the global eigenvalue problem given in Eq. (4), the eigenvalues related to the Lagrange multipliers $\boldsymbol{\mu}$ are non-physically infinite. When original FE models are reduced using the original and improved DCB methods in Eq. (17) and (30), respectively, such non-physical eigenvalues related to $\boldsymbol{\mu}$ and $\boldsymbol{\psi}$ $(\boldsymbol{\psi} = \lambda\boldsymbol{\mu})$ become finite, but appear in higher modes. The modes related to the additional coordinates can be eliminated through a further reduction using SEREP.

From the reduced system matrices in Eq. (30), the following eigenvalue problem is obtained:

$$\bar{\mathbf{K}}_2(\bar{\boldsymbol{\varphi}})_i = \bar{\lambda}_i \bar{\mathbf{M}}_2(\bar{\boldsymbol{\varphi}})_i, \quad i = 1, \cdots, N_2, \tag{31}$$

where $\bar{\lambda}_i$ and $(\bar{\boldsymbol{\varphi}})_i$ are the i-th eigenvalue and the corresponding mode vector, respectively. We then calculate the eigenvectors up to the N_1-th mode and construct the following eigenvector matrix

$$\bar{\boldsymbol{\Phi}} = \begin{bmatrix} (\bar{\boldsymbol{\varphi}})_1 & (\bar{\boldsymbol{\varphi}})_2 & \cdots & (\bar{\boldsymbol{\varphi}})_{N_1} \end{bmatrix}. \tag{32}$$

The transformation matrix of the improved DCB method is further reduced using the eigenvector matrix in Eq. (32) as follows.

$$\hat{\mathbf{T}}_2 = \mathbf{T}_2 \bar{\boldsymbol{\Phi}}, \tag{33}$$

and thus the new transformation matrix $\hat{\mathbf{T}}_2$ has the same size as $\mathbf{T}_1$ in the original DCB method $(N_g \times N_1)$. That is, the additional coordinate vector $\boldsymbol{\psi}$ is eliminated.

Finally, the resulting reduced system matrices are calculated as follows:

$$\hat{\mathbf{M}}_2 = \hat{\mathbf{T}}_2^T \begin{bmatrix} \mathbf{M} & \mathbf{0} \\ \mathbf{0} & \mathbf{0} \end{bmatrix} \hat{\mathbf{T}}_2, \; \hat{\mathbf{K}}_2 = \hat{\mathbf{T}}_2^T \begin{bmatrix} \mathbf{K} & \mathbf{B} \\ \mathbf{B}^T & \mathbf{0} \end{bmatrix} \hat{\mathbf{T}}_2, \hat{\mathbf{f}}_2 = \hat{\mathbf{T}}_2^T \begin{bmatrix} \mathbf{f} \\ \mathbf{0} \end{bmatrix}, \tag{34}$$

in which $\hat{\mathbf{M}}_2$, $\hat{\mathbf{K}}_2$, and $\hat{\mathbf{f}}_2$ are the final reduced mass, stiffness matrices, and force vector, respectively. Then, the size of the reduced system matrices provided by the improved DCB method becomes equal to that by the original DCB method.

The reduced system becomes more accurate by improving the DCB formulation. The increase of computational cost is inevitable, but the computation of the 2nd order residual flexibility is effectively performed using Eq. (25). In the following sections, the accu-

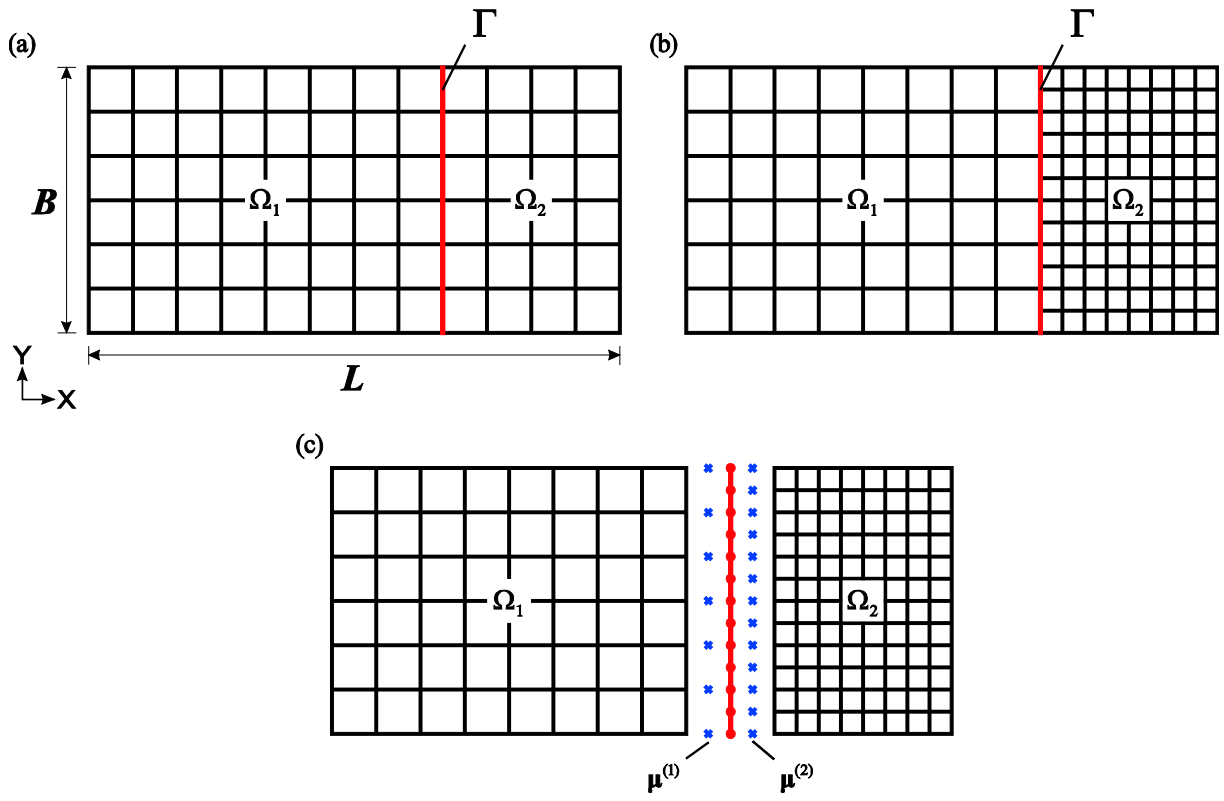

Fig. 2. Rectangular plate problem: (a) Matching mesh on the interface (12 × 6 mesh), (b) Non-matching mesh between neighboring substructures, (c) Interface boundary treatment.

racy and computational cost will be investigated using various numerical examples. In the numerical examples, the computation cost for the interface reduction process will also be examined.

4. Numerical examples

In this section, we investigate the performance of the improved DCB method compared to the original DCB method. We considered four structural problems: a rectangular plate with matching and non-matching meshes, a plate with a hole, a hyperboloid shell, and a bended pipe.

All finite element models are constructed using the 4-node MITC (Mixed Interpolation of Tensorial Components) shell elements [41–45], and free or fixed boundary conditions are imposed differently according to the problem. The frequency cut-off method is employed to select dominant substructural modes [39]. All the computer codes are implemented in MATLAB and computation is performed in a personal computer (Inter core (TM) i7-4770, 3.40 GHz CPU, 16 GB RAM).The relative eigenfrequency error is adopted to measure the accuracy of the reduced models

$$\xi_i = \frac{|\omega_i - \hat{\omega}_i|}{\omega_i}, \ \hat{\omega}_i = \sqrt{\hat{\lambda}_i} \tag{35}$$

in which ξ_i is the i-th relative eigenfrequency error, ω_i is the i-th exact eigenfrequency calculated from the global eigenvalue problem in Eq. (4); and $\hat{\omega}_i$ and $\hat{\lambda}_i$ are the i-th approximated eigenfrequency and eigenvalue calculated from the reduced eigenvalue problem. Note that the rigid body modes are not considered in measuring the accuracy.

4.1. Rectangular plate problem

Let us consider a rectangular plate with free boundary, see Fig. 2. Length L is 0.6096 m, width B is 0.3048 m, and thickness h is 3.18×10^{-3} m. Young's modulus E is 72 GPa, Poisson's ratio ν is 0.33, and density ρ is 2796 kg/m^3. The whole structure is an assemblage of two substructures ($N_s = 2$) modeled by 4-node MITC shell elements. We consider two numerical cases, with matching and non-matching meshes between neighboring substructures.

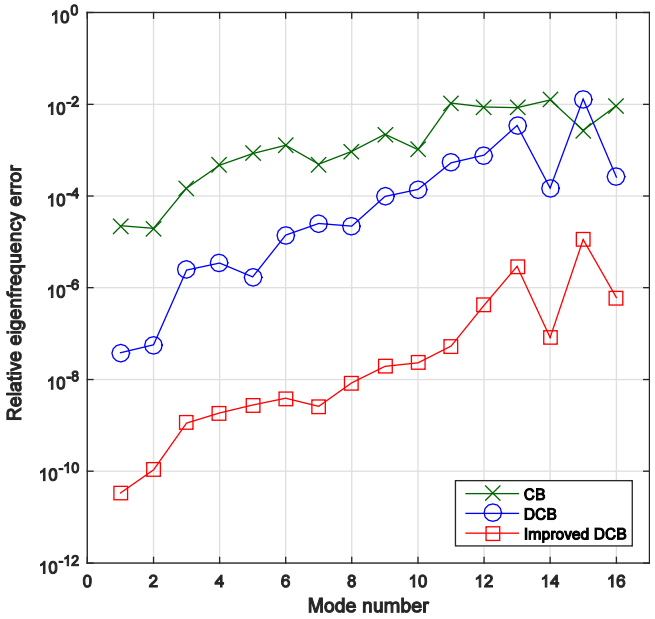

Fig. 3. Relative eigenfrequency errors in the rectangular plate problem with matching mesh in Fig. 2a.

Table 1
Number of dominant modes used and number of DOFs in original and reduced systems for the rectangular plate problem (12×6 mesh).

Methods	$N_d^{(1)}$	$N_d^{(2)}$	N_d	N_g	N_1
CB	13	7	20	455	55
DCB	13	7	20	525	67
Improved DCB	13	7	20	525	67

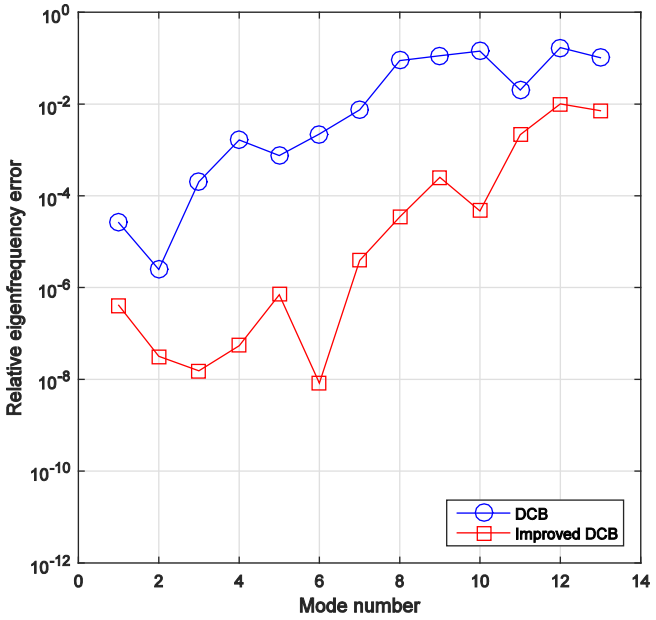

Fig. 4. Relative eigenfrequency errors in the rectangular plate problem with non-matching mesh in Fig. 2b.

For the matching mesh case, the first substructure is modeled using an 8×6 mesh and the second substructure is modeled using a 4×6 mesh, as shown in Fig. 2a. Fig. 3 presents the relative eigenfrequency errors obtained by the CB, the original and improved DCB methods. The numbers of dominant modes used and the numbers of DOFs in original and reduced systems are listed in Table 1. The improved DCB method shows significantly improved accuracy compared to the original CB method.

Let us consider the non-matching mesh case, see Fig. 2b. The first substructure is modeled by an 8×6 mesh and the second substructure is modeled by an 8×12 mesh. In this case, the interface compatibility is considered through nodal collocation and thus the matrices $\mathbf{B}^{(i)}$ are no longer Boolean, see Fig. 2c. Fig. 4 presents the relative eigenfrequency errors obtained by the original and improved DCB methods. Table 2 shows the numbers of dominant modes used and the numbers of DOFs in the original and reduced systems. The results also show that the improved method provides considerably more-accurate solutions for this non-matching mesh case.

Table 2
Number of dominant modes used and number of DOFs in original and reduced systems for the rectangular plate problem with non-matching mesh.

Methods	$N_d^{(1)}$	$N_d^{(2)}$	N_d	N_g	N_1
DCB	5	3	8	965	85
Improved DCB	5	3	8	965	85

4.2. Plate structure with a hole

Let us consider a rectangular plate with a hole, see Fig. 5. No boundary condition is imposed. The length L is 20 m, width B is 10 m, and thickness h is 0.25 m. Young's modulus E is 210 GPa, Poisson's ratio ν is 0.3, and density ρ is 7850 kg/m^3. The whole model is an assemblage of four substructural FE models ($N_s = 4$). The whole model is discretized by 208 shell elements (1360 DOFs). The substructures are symmetrically positioned about the hole in center.

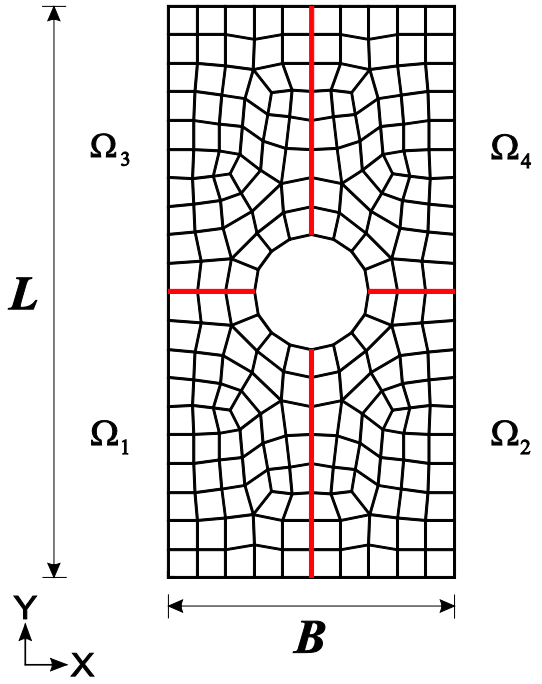

Fig. 5. Plate structure with a hole.

Table 3
Number of dominant modes used and number of DOFs in original and reduced systems for the plate structure with a hole.

Methods	$N_d^{(1)}$	$N_d^{(2)}$	$N_d^{(3)}$	$N_d^{(4)}$	N_d	N_g	N_1
DCB	5	5	5	5	20	1490	174
Improved DCB	5	5	5	5	20	1490	174

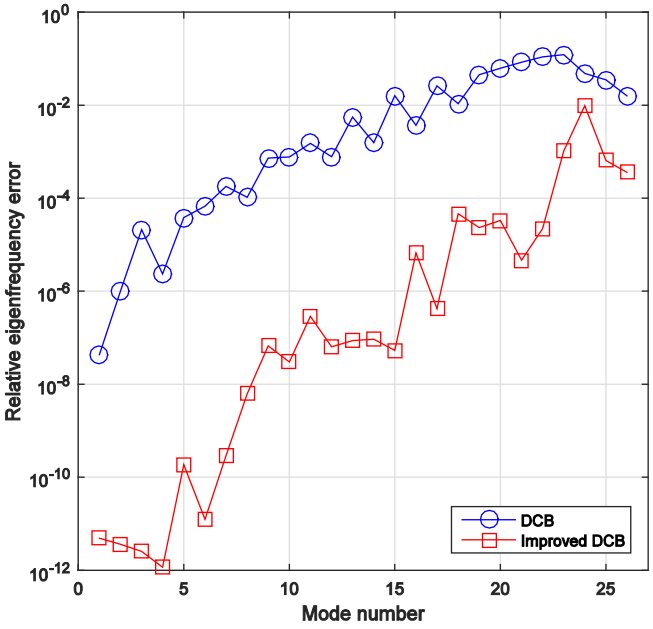

Fig. 6. Relative eigenfrequency errors in the plate structure with a hole.

The numbers of dominant modes used and the numbers of DOFs in the original and reduced systems are presented in Table 3. Fig. 6 presents the relative eigenfrequency errors obtained using the original and improved DCB methods. The results show that the improved DCB method largely outperforms the original DCB method, especially, in lower modes.

4.3. Hyperboloid shell problem

We here consider a hyperboloid shell structure with free boundary as shown in Fig. 7. Height H is 4.0 m and thickness h is 0.05 m. Young's modulus E is 69 GPa, Poisson's ratio ν is 0.35, and density ρ is 2700 kg/m^3. The mid-surface of this shell structure is described by

$$x^2 + y^2 = 2 + z^2; \quad z \in [-2, 2]. \tag{36}$$

Three substructures ($N_s = 3$) are assembled to construct the original FE model of the shell structures, in which 800 shell elements and 903 nodes are used (4200 DOFs). Table 4 lists the numbers of dom-

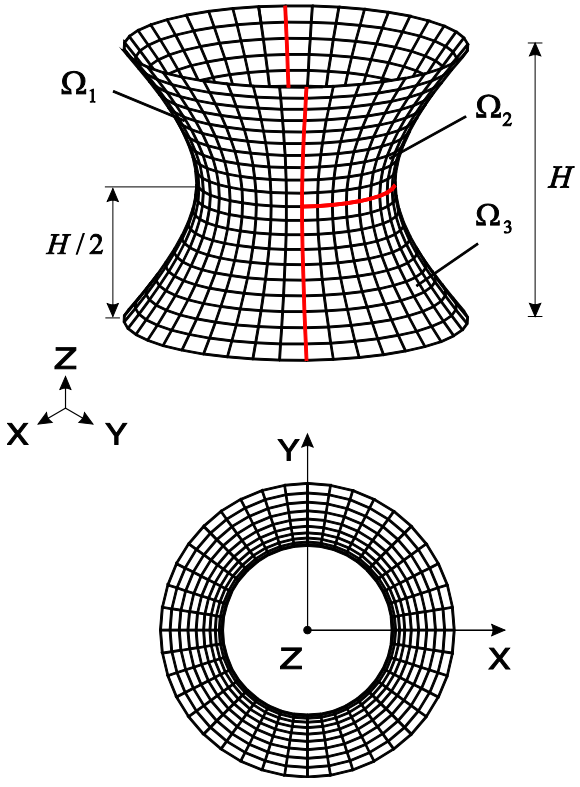

Fig. 7. Hyperboloid shell problem.

Table 4
Number of dominant modes used and number of DOFs in original and reduced systems for the hyperboloid shell problem.

Methods	$N_d^{(1)}$	$N_d^{(2)}$	$N_d^{(3)}$	N_d	N_g	N_1
DCB	10	10	10	30	4830	363
Improved DCB	10	10	10	30	4830	363

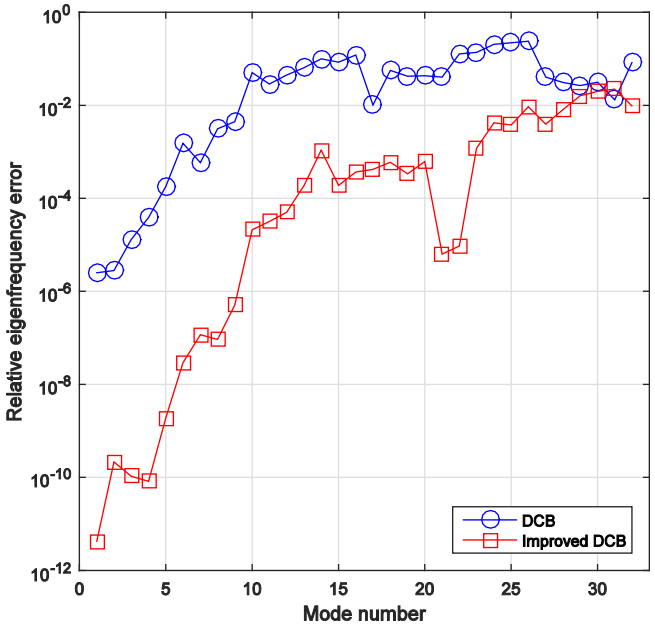

Fig. 8. Relative eigenfrequency errors in the hyperboloid shell problem.

Table 5
Computational costs for the hyperboloid shell problem in Fig. 8.

Methods	Items	Computation times	
		[sec]	Ratio [%]
Original DCB method	Substructural mode matrices ($\mathbf{R}^{(i)}$, $\mathbf{\Theta}_d^{(i)}$)	0.28	1.77
	Substructural 1st order residual flexibility matrices ($\mathbf{F}_1^{(i)}$)	15.11	96.94
	Reduced system matrices ($\bar{\mathbf{M}}_1$, $\bar{\mathbf{K}}_1$)	0.20	1.29
	Total	15.59	100.00
Improved DCB method	Substructural mode matrices ($\mathbf{R}^{(i)}$, $\mathbf{\Theta}_d^{(i)}$)	0.28	1.77
	Substructural 1st order residual flexibility matrices ($\mathbf{F}_1^{(i)}$)	15.11	96.94
	Substructural 2nd order residual flexibility matrices ($\mathbf{F}_2^{(i)}$)	0.36	2.31
	Reduced system matrices ($\bar{\mathbf{M}}_2$, $\bar{\mathbf{K}}_2$)	0.42	2.67
	Subtotal	16.17	103.69
	Interface reduction ($\hat{\mathbf{M}}_2$, $\hat{\mathbf{K}}_2$)	2.06	13.25
	Total	18.23	116.94

inant modes used and the numbers of DOFs in the original and reduced systems. Fig. 8 presents the relative eigenfrequency errors obtained using the original and improved DCB methods. The graphs in the figure consistently show the accuracy of the improved DCB method.

For this problem, we also compare the computational costs of the original and improved DCB methods. Table 5 shows the detailed computational costs. Compared to the original DCB method, the additional computation time required by the improved DCB method is 3.69% for accuracy improvement, and 13.25% for interface reduction.

4.4. Bended pipe problem

A bended pipe structure with clamped boundary at one end is considered as shown in Fig. 9, in which the structural configuration and specification are illustrated. Young's modulus E is 69 GPa, Poisson's ratio ν is 0.35, and density ρ is 2700 kg/m^3. The FE model of the pipe structure is an assemblage of three substructural FE models ($N_s = 3$). The whole FE model has 2511 shell elements and 2592 nodes (12960 DOFs).

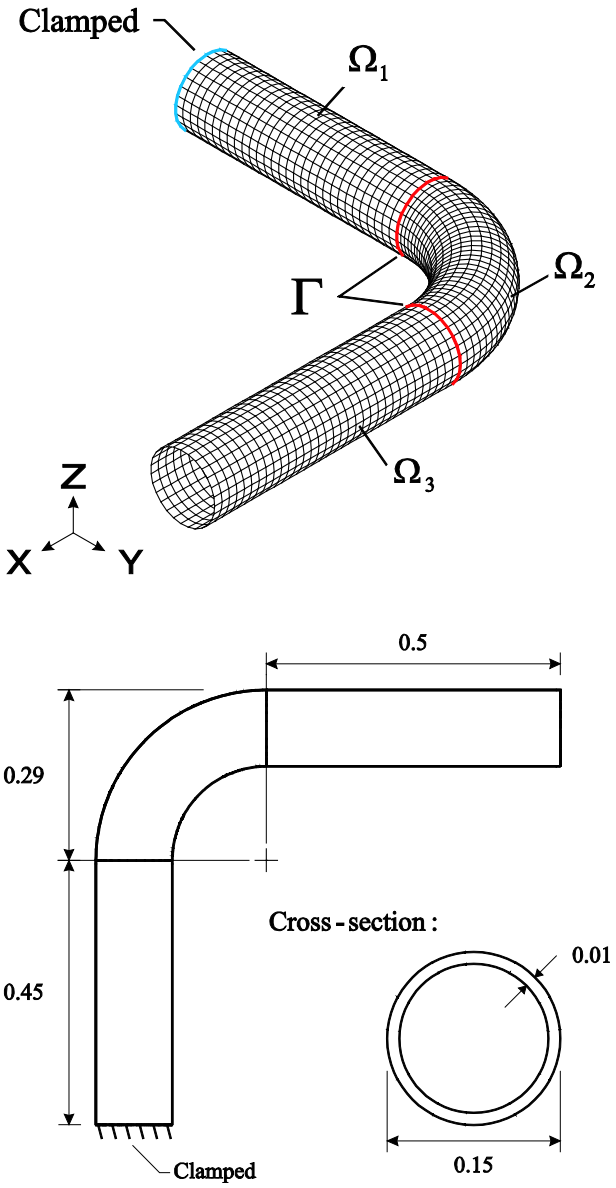

Fig. 9. Bended pipe problem.

Table 6
Number of dominant modes used and number of DOFs in the original and reduced systems for the bended pipe problem.

Methods	$N_d^{(1)}$	$N_d^{(2)}$	$N_d^{(3)}$	N_d	N_g	N_1
DCB	5	5	5	15	13,095	297
DCB	95	95	95	285	13,095	567
Improved DCB	5	5	5	15	13,095	297

The following numerical cases are considered:

- The original DCB method is used with the reduced model size of $N_1 = 297$ ($N_d = 15$) and $N_1 = 567$ ($N_d = 285$).
- The improved DCB method is used with the reduced model size of $N_1 = 297$ ($N_d = 15$).

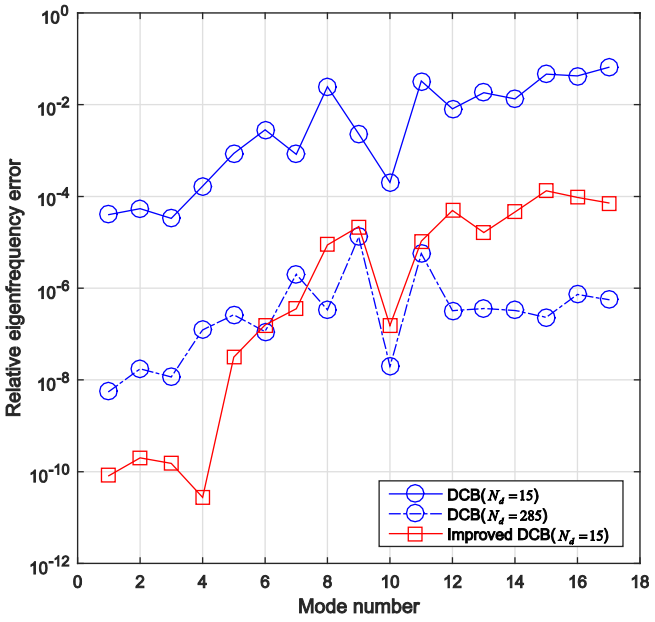

Fig. 10. Relative eigenfrequency errors in the bended pipe problem.

Table 7
Computational costs for the bended pipe problem in Fig. 10.

Methods	Items	Computation times	
		[sec]	Ratio [%]
Original DCB method ($N_d = 15$)	Substructural mode matrices ($\mathbf{R}^{(i)}$, $\mathbf{\Theta}_d^{(i)}$)	0.67	0.26
	Substructural 1st order residual flexibility matrices ($\mathbf{F}_1^{(i)}$)	256.40	99.44
	Reduced system matrices ($\bar{\mathbf{M}}_1$, $\bar{\mathbf{K}}_1$)	0.77	0.30
	Total	257.84	100.00
Original DCB method ($N_d = 285$)	Substructural mode matrices ($\mathbf{R}^{(i)}$, $\mathbf{\Theta}_d^{(i)}$)	3.61	1.40
	Substructural 1st order residual flexibility matrices ($\mathbf{F}_1^{(i)}$)	272.71	105.77
	Reduced system matrices ($\bar{\mathbf{M}}_1$, $\bar{\mathbf{K}}_1$)	0.81	0.31
	Total	277.13	107.48
Improved DCB method ($N_d = 15$)	Substructural mode matrices ($\mathbf{R}^{(i)}$, $\mathbf{\Theta}_d^{(i)}$)	0.67	0.26
	Substructural 1st order residual flexibility matrices ($\mathbf{F}_1^{(i)}$)	256.40	99.44
	Substructural 2nd order residual flexibility matrices ($\mathbf{F}_2^{(i)}$)	4.58	1.78
	Reduced system matrices ($\bar{\mathbf{M}}_2$, $\bar{\mathbf{K}}_2$)	1.46	0.57
	Subtotal	263.11	102.05
	Interface reduction ($\hat{\mathbf{M}}_2$, $\hat{\mathbf{K}}_2$)	1.29	0.50
	Total	264.40	102.55

The number of dominant modes used and the number of DOFs in the original and reduced systems are listed in Table 6.

Fig. 10 presents the relative eigenfrequency errors obtained by the original and improved DCB methods. When reduced models of the same size ($N_1 = 297$; $N_d = 15$) are considered, the improved DCB method provides a much more accurate reduced model. It is also observed that the original DCB method shows accuracy comparable to the improved DCB method when 285 modes are used for the original DCB. For similarly accurate reduced models, the model size obtained by the original DCB method ($N_1 = 567$) is almost twice that obtained by the improved DCB method ($N_1 = 297$).

Next, the computational costs of the original and improved DCB methods are compared. Table 7 shows the detailed computational costs. For reduced models of the same size, additional computation time required for the improved DCB method is 2.05% for accuracy improvement and 0.5% for interface reduction, compared to the original DCB method. The table also presents the detailed computation time when 285 modes are used for the original DCB method.

At this point, it is important to note that the improved DCB method is very useful for obtaining an accurate reduced model when only a limited number of dominant modes are available. Such cases happen when dominant modes are obtained experimentally.

Table 8
Eigenvalues calculated for the plate with a hole. Negative eigenvalues are underlined.

No.	Original DCB	Improved DCB
1	3.7518E+02	3.7517E+02
2	5.9356E+02	5.9306E+02
3	3.3397E+03	3.2415E+03
4	3.3609E+03	3.3549E+03
5	6.7871E+03	6.7483E+03
6	1.0588E+04	9.5708E+03
7	1.0631E+04	1.0252E+04
8	1.3618E+04	1.3502E+04
9	−1.8564E+04	2.1398E+04
10	−2.0246E+04	2.4833E+04
11	−2.3018E+04	3.7087E+04
12	2.7750E+04	3.8271E+04
13	−4.0962E+04	5.5247E+04
14	5.0359E+04	5.5684E+04
15	6.8518E+04	7.0494E+04
16	7.1921E+04	7.9612E+04
17	−7.3877E+04	8.0927E+04
18	−7.8759E+04	1.0925E+05
19	9.2383E+04	1.2573E+05
20	−1.0689E+05	1.2642E+05
21	−1.1249E+05	1.3012E+05
22	−1.4226E+05	1.8680E+05
23	−1.4899E+05	2.1227E+05
24	−1.5146E+05	2.3759E+05
25	−2.2205E+05	2.4295E+05

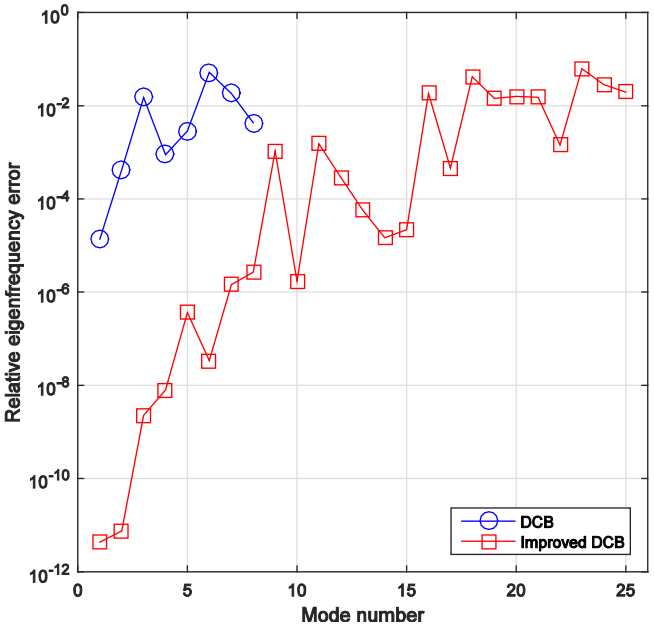

Fig. 11. Relative eigenfrequency errors in the plate structure with a hole ($N_d = 4$).

5. Negative eigenvalues in lower modes

In the previous section, we demonstrated that the accuracy of the DCB method was significantly improved. When the improved DCB method is used, it is expected that spurious modes will be avoided in lower modes, when the selected dominant modes in the substructure are insufficient. Spurious modes in the reduced model could cause instability in various dynamic analyses. There have been several attempts to prevent this [14,15].

In this section, we compare the improved DCB method with the original DCB method for the ability to avoid negative eigenvalues and the corresponding spurious modes in lower modes. The plate with a hole in Fig. 5 is considered again. Only one vibration mode is selected in each substructure ($N_d = 4$); thus, the reduction basis is not well established. The number of DOFs in both reduced systems (N_1) is 158. Note that the rigid body modes are not considered for investigating spurious modes.

The first 25 eigenvalues calculated are listed in Table 8, in which mode numbers are sorted by the magnitude of eigenvalues. Fig. 11 presents the relative eigenfrequency errors in the FE models reduced by the original and improved DCB methods, in which only eigenfrequencies corresponding to positive eigenvalues are plotted. The first negative eigenvalue obtained by the original DCB method is found at the 9th mode and, after that, 40 negative eigenvalues appear until the 57th mode. That is, many spurious modes are calculated in lower modes. Eigenvalues obtained are infinite from the 58th to 152th modes. However, when the improved DCB method is used, the first negative eigenvalue is found at the 51th modes and no infinite eigenvalue is calculated. That is, the appearance of negative eigenvalues is shifted to relatively higher frequency range. This is an advantageous feature of the improved DCB method.

6. Conclusions

In this study, we proposed a new CMS method by improving the DCB method. The formulation was derived by considering the second order effect of residual substructural modes. The transformation matrix of the original DCB method was enhanced by using the additional dynamic terms, and the resulting additional interface coordinates in the reduced system was eliminated by applying the concept of SEREP. An important feature of the improved DCB method lies in the fact that the accuracy of reduced models is remarkably improved and negative eigenvalues are avoided in lower modes. Through various numerical examples, we demonstrated accuracy and computational efficiency of the improved DCB method compared to the original DCB method.

In future work, it would be valuable to develop an effective parallel computation algorithm for the present method to deal with FE models with a large number of substructures and DOFs. We expect that the new method is an attractive solution for constructing accurate reduced models for experimental-FE model correlation, FE model updating, and optimizations.

Acknowledgements

This work was supported by the Basic Science Research Program through the National Research Foundation of Korea (NRF) funded by the Ministry of Science, ICT & Future Planning (No. 2014R1A1A1A05007219), and the grant (MPSS-CG-2015-01) through the Disaster and Safety Management Institute funded by Ministry of Public Safety and Security of Korean government.

References

[1] Hurty WC. Dynamic analysis of structural systems using component modes. AIAA J 1965;3(4):678–85.
[2] Kammer DC, Triller MJ. Selection of component modes for Craig-Bampton substructure representations. AIAA J 1996;118(2):264–70.
[3] Givoli D, Barbone PE, Patlashenko I. Which are the important modes of a subsystem? Intl J Numer Methods Eng 2004;59(2):1657–78.
[4] Liao BS, Bai Z, Gao W. The important modes of subsystems: a moment-matching approach. Intl J Numer Methods Eng 2007;70(13):1581–97.
[5] Craig RR, Bampton MCC. Coupling of substructures for dynamic analysis. AIAA J 1968;6(7):1313–9.
[6] Benfield WA, Hruda RF. Vibration analysis of structures by component mode substitution. AIAA J 1971;9:1255–61.
[7] MacNeal RH. Hybrid method of component mode synthesis. Comput Struct 1971;1(4):581–601.
[8] Rubin S. Improved component-mode representation for structural dynamic analysis. AIAA J 1975;13(8):995–1006.
[9] Craig RR, Chang CJ. On the use of attachment modes in substructure coupling for dynamic analysis. 18st Structures, Structural Dynamics and Material Conference 1977;89–99.
[10] Qiu JB, Ying ZG, Williams FW. Exact modal synthesis techniques using residual constraint modes. Intl J Numer Methods Eng 1997;40(13):2475–92.
[11] Rixen DJ. A dual Craig-Bampton method for dynamic substructuring. J Comput Appl Math 2004;168(1–2):383–91.
[12] Géradin M, Rixen DJ. Mechanical vibrations: theory and application to structural dynamics. John Wiley & Sons; 2014.
[13] Park KC, Park YH. Partitioned component mode synthesis via a flexibility approach. AIAA J 2004;42(6):1236–45.
[14] Rixen DJ. Dual Craig-Bampton with enrichment to avoid spurious modes. Proceedings of the IMAC-XXVII Conference & Exposition on Structural Dynamics, Orlando, USA. 2009.
[15] Markovic D, Ibrahimbegovic A, Park KC. Partitioning based reduced order modelling approach for transient analyses of large structures. Eng Comput 2009;26(1/2):46–68.
[16] Perdahcıoğlu, Akçay D, et al. An optimization method for dynamics of structures with repetitive component patterns. Struct Multidisc Optim 2009;39(6):557–67.
[17] Voormeeren SN, De Klerk D, Rixen DJ. Uncertainty quantification in experimental frequency based substructuring. Mech Syst Signal PR 2010;24 (1):106–18.
[18] Voormeeren SN, Van Der Valk PLC, Rixen DJ. Generalized methodology for assembly and reduction of component models for dynamic substructuring. AIAA J 2011;49(5):1010–20.
[19] Rixen DJ, Boogaard A, van der Seijs MV, van Schothorst G, van der Poel T. Vibration source description in substructuring: a theoretical depiction. Mech Syst Signal PR 2015;60:498–511.
[20] Géradin M, Rixen DJ. A 'nodeless' dual superelement formulation for structural and multibody dynamics application to reduction of contact problems. Intl J Numer Methods Eng 2016;106:773–98.
[21] Brecher C, Fey M, Tenbrock C, Daniels M. Multipoint constraints for modeling of machine tool dynamics. J Manuf Sci E-T ASME 2016;138(5):051006.
[22] Blachowski B, Gutkowski W. Effect of damaged circular flange-bolted connections on behaviour of tall towers, modelled by multilevel substructuring. Eng Struct 2016;111:93–103.
[23] Bathe KJ, Jian Dong. Component mode synthesis with subspace iterations for controlled accuracy of frequency and mode shape solutions. Compt Struct 2014;139:28–32.
[24] Kim JG, Lee PS. An enhanced Craig-Bampton method. Intl J Numer Methods Eng 2015;103:79–93.
[25] Kim JG, Boo SH, Lee PS. An enhanced AMLS method and its performance. Comput Methods Appl Mech Eng 2015;287:90–111.
[26] Boo SH, Kim JG, Lee PS. A simplified error estimator for the CB method and its application to error control. Compt Struct 2016;164:53–62.
[27] Boo SH, Kim JG, Lee PS. Error estimation method for automated multi-level substructuring method. Intl J Numer Methods Eng 2015. http://dx.doi.org/10.1002/nme.5161.
[28] Boo SH, Lee PS. A dynamic condensation method using algebraic substructuring. Intl J Numer Methods Eng 2016. http://dx.doi.org/10.1002/nme.5349.
[29] Kim JM. Development of a component mode synthesis method with higher-order residual flexibility [M.S. thesis]. Department of Mechanical Engineering, KAIST; 2016.
[30] Baek SM. Study on the multi-level substructuring scheme and system condensation for the large-scaled structural dynamic analysis [Ph.D. thesis]. Department of Mechanical and Aerospace Engineering, Seoul National University; 2012.
[31] Kadawathagedara SW, Rixen DJ. Model reduction in co-rotated multi-body dynamics based on the dual Craig-Bampton method. 52nd AIAA/ASME/ASCE/AHS/ASC Structures, Structural Dynamics and Materials Conference, Denver, USA, 4–7 April 2011;2011–2029.
[32] Hinke L, Dohnal F, Mace BR, Waters TP, Ferguson NS. Component mode synthesis as a framework for uncertainty analysis. J Sound Vib 2009;324 (1):161–78.

[33] Papadimitriou C, Papadioti DC. Component mode synthesis techniques for finite element model updating. Comput Struct 2013;126:15–28.
[34] Qu, ZQ. Model order reduction techniques with applications in finite element analysis. Springer Science & Business Media; 2013.
[35] O'Callahan J. A procedure for an improved reduced system (IRS) model. In: Proceedings of the 7th international modal analysis conference, Las Vegas; 1989. p. 17–21.
[36] O'Callahan J, Avitabile P, Riemer R. System equivalent reduction expansion process (SEREP). In: Proceedings of the 7th International Modal Analysis Conference, Las Vegas; 1989. p. 29–37.
[37] Golub GH, Van Loan CF. Matrix computations. 4th ed. JHU Press; 2012. p. 304–7.
[38] Van der Sluis A. Stability of the solutions of linear least squares problems. Numerische Mathematik J 1974;23(3):241–54.
[39] Hurty WC. A criterion for selecting realistic natural modes of a structure. Pasadena, CA: Technical Memorandum, Jet Propulsion Laboratory; 1967. p. 33–364.
[40] Craig RR, Kurdila AJ. Fundamentals of structural dynamics. John Wiley & Sons; 2006.
[41] Bathe KJ. Finite element procedure; 2006.
[42] Bathe KJ, Dvorkin EN. A formulation of general shell elements – the use of mixed interpolation of tensorial components. Intl J Numer Methods Eng 1986;22(3):697–722.
[43] Lee PS, Bathe KJ. Development of MITC isotropic triangular shell finite elements. Comput Struct 2004;82(11–12):945–62.
[44] Lee Y, Lee PS, Bathe KJ. The MITC3+ shell finite element and its performance. Comput Struct 2014;138:12–23.
[45] Lee Y, Jeon HM, Lee PS, Bathe KJ. The modal behavior of the MITC3+ triangular shell element. Comput Struct 2015;153:148–64.